Speciated atmospheric mercury and sea-air exchange of gaseous mercury in the South China Sea

Chunjie Wang[1], Zhangwei Wang[1], Fan Hui[2], Xiaoshan Zhang[1]

[1] Research Center for Eco-Environmental Sciences, Chinese Academy of Sciences, 18 Shuangqing Road, Beijing, China

[2] China University of Petroleum (Beijing), 18 Fuxue Road, Beijing, China

Correspondence to: Xiaoshan Zhang (zhangxsh@rcees.ac.cn)

Abstract

The characteristics of the reactive gaseous mercury (RGM) and particulate mercury (Hg^P) in the marine boundary layer (MBL) is poorly understood due in part to sparse data from sea and ocean. Gaseous elemental Hg (GEM), RGM and size-fractioned Hg^P in marine atmosphere, and dissolved gaseous Hg (DGM) in surface seawater were determined in the South China Sea (SCS) during an oceanographic expedition (3–28 September 2015). The mean concentrations of GEM, RGM and $Hg^P_{2.5}$ were 1.52 ± 0.32 ng m^{-3}, 6.1 ± 5.8 pg m^{-3} and 3.2 ± 1.8 pg m^{-3}, respectively. Low GEM level indicated that the SCS suffered less influence from fresh emissions, which could be due to the majority of air masses coming from the open oceans as modeled by backward trajectories. Atmospheric reactive Hg (RGM + $Hg^P_{2.5}$) represented less than 1 % of total atmospheric Hg, indicating that atmospheric Hg existed mainly as GEM in the MBL. The GEM and RGM concentrations (1.73 ± 0.40 ng m^{-3} and 7.1 ± 1.4 pg m^{-3} respectively) in the northern SCS were significantly higher than those (1.41 ± 0.26 ng m^{-3} and 3.8 ± 0.7 pg m^{-3}) in the western SCS, and the $Hg^P_{2.5}$ and Hg^P_{10} levels (8.3 and 24.4 pg m^{-3}) in the Pearl River Estuary (PRE) were 0.5–6.0 times higher than those in the open waters of the SCS, indicating that the PRE was polluted to some extent. The size distribution of Hg^P in PM_{10} was observed to be three-modal with peaks around <0.4 μm, 0.7–1.1 μm and 5.8–9.0 μm, respectively, but the coarse modal was the dominant size, especially in the open SCS. There was no significant diurnal variation of GEM and $Hg^P_{2.5}$, but we found the RGM concentrations were significantly higher in daytime (8.0 ± 5.5 pg m^{-3}) than in nighttime (2.2 ± 2.7 pg m^{-3}) mainly due to the influence of solar radiation. In the northern SCS, the DGM concentrations in nearshore area (40−55 pg l^{-1}) were about twice as high as those in the open sea, but this pattern was not significant in the western SCS. The sea-air exchange fluxes of Hg^0 in the SCS varied from 0.40 to 12.71 ng m^{-2} h^{-1} with a mean value of 4.99 ± 3.32 ng m^{-2} h^{-1}. The annual emission flux of Hg^0 from the SCS to the atmosphere was estimated to be 159.6 tons yr^{-1}, accounting for about 5.54 % of the global Hg^0 oceanic evasion though the SCS only represents 1.0 % of the global ocean area. Additionally, the annual dry deposition flux of atmospheric reactive Hg represented more than 18 % of the annual evasion flux of Hg^0, and

therefore the dry deposition of atmospheric reactive Hg was an important pathway for the input of atmospheric Hg to the SCS.

1 Introduction

Mercury (Hg) is a naturally occurring metal. Hg is released to the environment through both the natural and anthropogenic pathways (Schroeder and Munthe, 1998). However, since the Industrial Revolution, the anthropogenic emissions of Hg increased drastically. Continued rapid industrialization has made Asia the largest source region of Hg emissions to air, with East and Southeast Asia accounting for about 40 % of the global total (UNEP, 2013). Three operationally defined Hg forms are present in the atmosphere: gaseous elemental Hg (GEM or Hg^0), reactive gaseous Hg (RGM) and particulate Hg (Hg^P) (Schroeder and Munthe, 1998; Landis et al., 2002), while they have different physicochemical characteristics. It should be noted that all of the acronyms in this article have been listed in the Appendix. GEM is very stable with a residence time of 0.2–1.0 yr due to its high volatility and low solubility (Radke et al., 2007; Selin et al., 2007; Horowitz et al., 2017). Therefore, GEM can be transported for a long-range distance in the atmosphere, and this makes it well-mixed on a regional and global scale. Generally, GEM makes up more than 95 % of total atmospheric Hg (TAM), while the RGM and Hg^P concentrations (collectively known as atmospheric reactive mercury) are typically 2–3 orders of magnitude smaller than GEM in part because they are easily removed from ambient air by wet and dry deposition (Laurier and Mason, 2007; Holmes et al., 2009; Gustin et al., 2013), and they can also be reduced back to Hg^0.

Numerous previous studies have shown that Hg^0 in the marine boundary layer (MBL) can be rapidly oxidized to form RGM in situ (Laurier et al., 2003; Sprovieri et al., 2003, 2010; Laurier and Mason, 2007; Soerensen et al., 2010a; Wang et al., 2015; Mao et al., 2016; Ye et al., 2016). Ozone and OH could potentially be important oxidants on aerosols (Ariya et al., 2015; Ye et al., 2016), while the reactive halogen species (e.g., Br, Cl and BrO, generating from sea salt aerosols) may be the dominant sources for the oxidation of Hg^0 in the MBL (Holmes et al., 2006, 2010; Auzmendi-Murua et al., 2014; Gratz et al., 2015; Steffen et al., 2015; Shah et al., 2016; Horowitz et al., 2017). However, a recent study showed that Br and BrO became dominant GEM oxidants in the marine atmosphere with mixing ratios reaching 0.1 and 1 pptv, respectively, and contributing ~ 70 % of the total RGM production during midday, while O_3 dominated GEM oxidation (50–90 % of RGM production) when Br and BrO mixing ratios were diminished (Ye et al., 2016). The wet and dry deposition (direct or uptake by sea-salt aerosol) represents a major input of RGM and Hg^P to the sea and ocean due to their special and unique characteristics (i.e., high reactivity and water solubility) (Landis et al., 2002; Holmes et al., 2009). Previous studies also showed that atmospheric wet and dry deposition of RGM (mainly $HgBr_2$, $HgCl_2$, HgO, Hg-nitrogen and sulfur compounds) was the greatest source of Hg to open oceans (Holmes et al., 2009; Mason et al., 2012;

Huang et al., 2017). A recent study suggested that approximately 80 % of atmospheric reactive Hg sinks into the global oceans, and most of the deposition takes place to the tropical oceans (Horowitz et al., 2017).

The atmospheric reactive Hg deposited to the oceans follows different reaction pathways. One important process is that divalent Hg can be combined with the existing particles followed by sedimentation, or be converted to methylmercury (MeHg), the most bioaccumulative and toxic form of Hg in seafood (Ahn et al., 2010; Mason et al., 2017). Another important process is that the divalent Hg can be converted to dissolved gaseous Hg (DGM) through abiotic and biotic mechanisms (Strode et al., 2007). It is well known that almost all DGM in the surface seawater is Hg^0 (Horvat et al., 2003), while the dimethylmercury is extremely rare in the surface seawater (Bowman et al., 2015). It has been found that a majority of the surface seawater was supersaturated with respect to Hg^0 (Soerensen et al., 2010b, 2013, 2014), and parts of this Hg^0 may be emitted to the atmosphere. Evasion of Hg^0 from the oceanic surface into the atmosphere is partly driven by the solar radiation and aquatic Hg pools of natural and anthropogenic origins (Andersson, et al., 2011). Sea-air exchange is an important component of the global Hg cycle as it mediates the rate of increase in ocean Hg and therefore the rate of change in level of MeHg. Consequently, Hg^0 evasion from sea surface not only decreases the amount of Hg available for methylation in waters but also has an important effect on the redistribution of Hg in the global environment (Strode et al., 2007).

In recent years, speciated atmospheric Hg has been monitored in coastal areas (Xu et al., 2015; Ye et al., 2016; Howard et al., 2017; Mao et al., 2017) and open seas and oceans (e.g., Chand et al., 2008; Soerensen et al., 2010a; Mao et al., 2016; Wang et al., 2016a, b). However, there exists a dearth of knowledge regarding speciated atmospheric Hg and sea-air exchange of Hg^0 in tropical seas, such as the South China Sea (SCS). The highly time-resolved ambient GEM concentrations were measured using a Tekran® system. Simultaneously, the RGM, Hg^P and DGM were measured using manual methods. The main objectives of this study are to identify the spatial-temporal characteristics of speciated atmospheric Hg and to investigate the DGM concentrations in the SCS during the cruise, and then to calculate the Hg^0 flux based on the meteorological parameters as well as the concentrations of GEM in air and DGM in surface seawater. These results will raise our knowledge of the Hg cycle in tropical marine atmosphere and waters.

2 Materials and methods

2.1 Study area

The SCS is located in the downwind of Southeast Asia (Fig. 1a), and it is the largest semi-enclosed marginal sea in the western tropical Pacific Ocean. The SCS is connected with the East China Sea (ECS) to the northeast and the western Pacific Ocean to the east (Fig. 1a). The SCS is surrounded

by numerous developing and developed countries (Fig. 1a). An open cruise was organized by the South China Sea Institute of Oceanology (Chinese Academy of Sciences) and conducted during the period of 3–28 September 2015. The sampling campaign was conducted on R/V *Shiyan 3*, which departed from Guangzhou, circumnavigated the northern and western SCS and then returned to Guangzhou. The DGM sampling stations and R/V tracks are plotted in Fig. 1b. In this study, meteorological parameters (including photosynthetically available radiation (PAR) (Li-COR®, Model: Li-250), wind speed, air temperature and RH) were measured synchronously with atmospheric Hg onboard the R/V.

2.2 Experimental methods

2.2.1 Atmospheric GEM measurements

In this study, GEM was measured using an automatic dual channel, single amalgamation cold vapor atomic fluorescence analyzer (Model 2537B, Tekran®, Inc., Toronto, Canada), which has been reported in our previous studies (Wang et al., 2016a, b, c). In order to reduce the contamination from ship exhaust plume as possible, we installed the Tekran® system inside the ship laboratory (the internal air temperature was controlled to 25 ℃ using an air conditioner) on the fifth deck of the R/V and mounted the sampling inlet at the front deck 1.5 m above the top deck (about 16 m above sea level) using a 7 m heated (maintained at 50 ℃) polytetrafluoroethylene (PTFE) tube (¼ inch in outer diameter). The sampling interval was 5 min and the air flow rate was 1.5 l min^{-1} in this study. Moreover, two PTFE filters (0.2 μm pore size, 47 mm diameter) were positioned before and after the heated line, and the soda lime before the instrument was changed every 3 days during the cruise. The Tekran® instrument was calibrated every 25 h using the internal calibration source and these calibrations were checked by injections of certain volume of saturated Hg^0 before and after this cruise. The relative percent difference between manual injections and automated calibrations was < 5 %. The precision of the analyzer was determined to > 97 %, and the detection limit was < 0.1 ng m^{-3}.

The meteorological and basic seawater parameters were collected onboard the R/V, which was equipped with meteorological and oceanographic instrumentations. To investigate the influence of air masses movements on the GEM levels, 72-h backward trajectories of air masses were calculated using the Hybrid Single Particle Lagrangian Integrated Trajectory (HYSPLIT) model (Draxler and Rolph, 2012) and TrajStat software (Wang et al., 2009) based on Geographic Information System. Global Data Assimilation System (GDAS) meteorological dataset (ftp://arlftp.arlhq.noaa.gov/pub/archives/gdas1/) with 1° × 1° latitude and longitude horizontal spatial resolution and 23 vertical levels at 6-h intervals was used as the HYSPLIT model input. It should be noted that the start time of each back trajectory was identical to the GEM sampling time (UTC) and the start height was set at 500 m above sea level to represent the approximate height of the mixing marine boundary layer where atmospheric pollutants were well mixed.

2.2.2 Sampling and analysis of RGM and Hg^P

The $Hg^P_{2.5}$ (Hg^P in $PM_{2.5}$) was collected on quartz filter (47 mm in diameter, Whatman), which has been reported in several previous studies (Landis et al., 2002; Liu et al., 2011; Kim et al., 2012;). It should be pointed out that the KCl coated denuders were heated at 500 ℃ for 1 h and the quartz filters were pre-cleaned by pyrolysis at 900 ℃ for 3 h to remove the possible pollutant. The RGM and $Hg^P_{2.5}$ were sampled using a manual system (URG-3000M), which has been reported in previous studies (Landis et al., 2002; Liu et al., 2011; Wang et al., 2016b). The sampling unit includes an insulated box (Fig. S1), two quartz annular denuders, two Teflon filter holder (URG Corporation) and a pump etc. The sampling flow rate was 10 l min^{-1} (Landis et al., 2002), and the sampling inlet was 1.2 m above the top deck of the R/V. In this study, one $Hg^P_{2.5}$ sample was collected in the daytime (6:00–18:00) and the other in the nighttime (18:00–6:00 (next day)), while two RGM samples were collected in the daytime (6:00–12:00 and 12:00–18:00, local time) and one RGM sample in the nighttime. Quality assurance and quality control for Hg^P and RGM were carried out using field blank samples and duplicates. The field blank denuders and quartz filters were treated similarly to the other samples but not sampling. The mean relative differences of duplicated $Hg^P_{2.5}$ and RGM samples (n = 6) were 13 ±6 % and 9 ±7 %, respectively.

Meanwhile, we collected different size particles using an Andersen impactor (nine-stage), which has been widely used in previous studies (Feddersen et al., 2012; Kim et al., 2012; Zhu et al., 2014; Wang et al., 2016a). The Andersen cascade impactor was installed on the front top deck of the R/V to sample the size-fractioned particles in PM_{10}. In order to diminish the contamination from exhaust plume of the ship as much as possible, we turned off the pump when R/V arrived at stations, and then switched back on when the R/V went to next station. The sample collection began in the morning (10:00 am) and continued for 2 days with a sampling flow rate of 28.3 l min^{-1}. Field blanks for Hg^P were collected by placing nine pre-cleaned quartz filters (81 mm in diameter, Whatman) in another impactor for 2 days without turning on the pump. After sampling, the quartz filters were placed in cleaned plastic boxes (sealing in Zip Lock plastic bags), and then were immediately preserved at −20 ℃ until the analysis.

The detailed analysis processes of RGM and Hg^P have been reported in our previous studies (Wang et al., 2016a, b). Briefly, the denuder and quartz filter were thermally desorbed at 500 ℃ and 900 ℃, respectively, and then the resulting thermally decomposed Hg^0 in carrier gas (zero air, i.e., Hg-free air) was quantified. The method detection limit was calculated to be 0.67 pg m^{-3} for RGM based on 3 times the standard deviation of the blanks (n = 57) for the whole dataset. The average field blank of denuders was 1.2 ± 0.6 pg (n = 6). The average blank values (n = 6) of $Hg^P_{2.5}$ and Hg^P_{10} were 1.4 pg (equivalent of < 0.2 pg m^{-3} for a 12 h sampling time) and 3.2 pg (equivalent of < 0.04 pg m^{-3} for a 2-day sampling time) of Hg per filter, respectively. The detection limits of $Hg^P_{2.5}$ and Hg^P_{10} were all less than 1.5 pg m^{-3} based on 3 times the standard deviation of field blanks. It should be noted that all the observed RGM and Hg^P values were

higher than the corresponding blank values, and the average blank values for RGM and Hg^P were subtracted from the samples.

2.2.3 Determination of DGM in surface seawater

In this study, the analysis was carried out according to the trace element clean technique, all containers (borosilicate glass bottles and PTFE tubes, joints and valves) were cleaned prior to use with detergent, followed by trace-metal-grade HNO_3 and HCl, and then rinsed with Milli-Q water (> 18.2 MΩ cm^{-1}), which has been described in our previous study (Wang et al., 2016c). DGM were measured in situ using a manual method (Fu et al., 2010; Ci et al., 2011). The detailed sampling and analysis of DGM has been elaborated in our previous study (Wang et al., 2016c). The analytical blanks were conducted onboard the R/V by extracting Milli-Q water for DGM. The mean concentration of DGM blank was 2.3 ± 1.2 pg l^{-1} (n = 6), accounting for 3–10 % of the raw DGM in seawater samples. The method detection limit was 3.6 pg l^{-1} on the basis of three times the standard deviation of system blanks. The relative standard deviation of duplicate samples generally < 8 % of the mean concentration (n = 6).

2.2.4 Estimation of sea-air exchange flux of Hg^0

The sea-air flux of Hg^0 was calculated using a thin film gas exchange model developed by Liss and Slater (1974) and Wanninkhof (1992). The detailed calculation processes of Hg^0 flux have been reported in recent studies (Ci et al., 2011; Kuss, 2014; Wang et al., 2016c; Kuss et al., 2018). It should be noted that the Schmidt number for gaseous Hg (Sc_{Hg}) is defined as the following equation: $Sc_{Hg} = v/D_{Hg}$, where v is the kinematic viscosity ($cm^2\ s^{-1}$) of seawater calculated using the method of Wanninkhof (1992), D_{Hg} is the Hg^0 diffusion coefficient ($cm^2\ s^{-1}$) in seawater, which is calculated according to the recent research (Kuss, 2014). The degree of Hg^0 saturation (S_a) was calculated using the following equation: $S_a = H'\ DGM_{conc.}/GEM_{conc}$, and the calculation of H' (the dimensionless Henry's Law constant) has been reported in previous studies (Ci et al., 2011, 2015; Kuss, 2014).

3 Results and discussion

3.1 Speciated atmospheric Hg concentrations

Figure 2 shows the time series of speciated atmospheric Hg and meteorological parameters during the cruise in the SCS. The GEM concentration during the whole study period ranged from 0.92 to 4.12 ng m^{-3} with a mean value of 1.52 ± 0.32 ng m^{-3} (n = 4673), which was comparable to the average GEM levels over the global oceans (1.4−1.6 ng m^{-3}, Soerensen et al., 2010a, 2013) and Atlantic Ocean (1.52 ± 0.32 ng m^{-3}, Laurier and Mason, 2007), and higher than those at background sites in the Southern Hemisphere (0.85−1.05 ng m^{-3}, Slemr et al., 2015; Howard et al., 2017), and also higher than those in remote oceans, such as the Cape Verde Observatory

station (1.19 ± 0.13 ng m^{-3}, Read et al., 2017), equatorial Pacific Ocean (1.15−1.05 ng m^{-3}, Soerensen et al., 2014) and Indian Ocean (1.0−1.2 ng m^{-3}, Witt et al., 2010; Angot et al., 2014), but lower than those in marginal seas, such as the Bohai Sea (BS), Yellow Sea (YS) and East China Sea (ECS) (Table 1). However, previous studies conducted in the northern SCS showed that the average GEM concentrations in their study period (2.6−3.5 ng m^{-3}, Fu et al., 2010; Tseng et al., 2012) were higher than that in this study. This is due to the fact that the GEM level in the northern SCS (Fu et al., 2010; Tseng et al., 2012) were considerably higher than that in the western SCS (this study).

The $Hg^{P}_{2.5}$ concentrations over the SCS ranged from 1.2 to 8.3 pg m^{-3} with a mean value of 3.2 ± 1.8 pg m^{-3} (n = 39) (Fig. 2), which was higher than those observed at Nam Co (China) and the Amsterdam Island, and were comparable to those in other coastal areas, such as the Okinawa Island, the Nova Scotia, the Adriatic Sea, the Ontario lake and the Weeks Bay (see Table 1), but lower than those in the BS and YS (Wang et al., 2016b), and considerably lower than those in rural and urban sites, such as Xiamen, Seoul (see Table 1), Guiyang and Waliguan (Fu et al., 2011, 2012). The results showed that the SCS suffered less influence from human activities. The RGM concentration over the SCS ranged from 0.27 to 27.57 pg m^{-3} with a mean value of 6.1 ± 5.8 pg m^{-3} (n = 58), which was comparable to those in other seas, such as the North Pacific Ocean, the North Atlantic Ocean and the Mediterranean Sea (including the Adriatic Sea) (Table 1), and higher than the global mean RGM concentration in the MBL (Soerensen et al., 2010a), and also higher than those measured at a few rural sites (Valente et al., 2007; Liu et al., 2010; Cheng et al., 2013, 2014), but significantly much lower than those polluted urban areas in China and South Korea, such as Guiyang (35.7 ± 43.9 pg m^{-3}, Fu et al., 2011), Xiamen, and Seoul (Table 1). Furthermore, Figure 2 shows that the long-lived GEM has smaller variability compared to the short-lived species like RGM and $Hg^{P}_{2.5}$, indicating that atmospheric reactive Hg was easily scavenged from the marine atmosphere due not only to their characteristics (high activity and solubility) but also due to their sensitivity to meteorological conditions and chemical environments. This pattern was consistent with our previous observed patterns in the BS and YS (Wang et al., 2016b). Moreover, we found that atmospheric reactive Hg represents less than 1 % of TAM in the atmosphere, which was comparable to those measured in other marginal and inner seas, such as the BS and YS (Wang et al., 2016b), Adriatic Sea (Sprovieri and Pirrone, 2008), Okinawa Island (located in the ECS) (Chand et al., 2008), but was significantly lower than those at the urban sites (Table 1).

3.2 Spatial distribution of atmospheric Hg

3.2.1 Spatial distributions of GEM and RGM

The spatial distribution of GEM over the SCS is illustrated in Fig. 3a. The mean GEM concentration in the northern SCS (1.73 ± 0.40 ng m^{-3} with a range of 1.01–4.12 ng m^{-3}) was significantly higher than that in the western SCS (1.41 ± 0.26 ng m^{-3} with a range of 0.92–2.83 ng

m^{-3}) (*t*-test, $p < 0.01$). Additionally, we found that the GEM concentrations in the PRE (the average value > 2.00 ng m^{-3}) were significantly higher than those in the open SCS (see Figs. 2, 3a), indicating that this nearshore area suffered from high GEM pollution in our study period probably due to the surrounding human activities. Figure 3a shows that there was large difference in GEM concentration between stations 1–10 and stations 16–31. The 72-h back-trajectories of air masses showed that the air masses with low GEM levels between stations 1 and 10 mainly originated from the SCS (Fig. S2a), while the air masses with high GEM levels at stations 16–31 primarily originated from East China and ECS, and then passed over the southeast coastal regions of China (Fig. S2b). Additionally, Fig. 3a shows that there was small variability of GEM concentrations over the western SCS except the measurements near the station 79. The back-trajectories showed that the air masses with elevated GEM level near the station 79 originated from the south of the Taiwan Island, while the other air masses mainly originated from the West Pacific Ocean (Fig. S3a) and the Andaman Sea (Fig. S3b). Therefore, the air masses dominantly originated from sea and ocean in this study period, and this could be the main reason for the low GEM level over the SCS. In conclusion, GEM concentrations showed a conspicuous dependence on the sources and movement patterns of air masses during this cruise.

The spatial distribution of RGM over the SCS is plotted in Fig. 3b. The mean RGM concentration in the northern SCS (7.1 ± 1.4 pg m^{-3}) was also obviously higher than that in the western SCS (3.8 ± 0.7 pg m^{-3}) (*t*-test, $p < 0.05$), indicating that a portion of RGM in the northern SCS maybe originated from the anthropogenic emission. We observed elevated RGM concentrations in the PRE, and which was consistent with the GEM distribution pattern, indicating that part of the RGM near PRE probably originated from the surrounding human activities. This is confirmed by the following fact: The RGM concentrations in nighttime of the two days in the PRE were 11.3 and 5.2 pg m^{-3} (Figs. 3b and S4), and they were significantly higher than those in the open SCS. Another obvious feature is that the amplitude of RGM concentration is much greater than the GEM, and this further indicated that the RGM was easily removed from the atmosphere through both the wet and dry deposition. In addition, we found that the RGM concentrations in the nearshore area were not always higher than those in the open sea except the measurements in the PRE, suggesting that the RGM in the remote marine atmosphere presumably not originated from land but from the in situ photo-oxidation of Hg^0, which had been reported in previous studies (e.g., Hedgecock and Pirrone, 2001; Lindberg et al., 2002; Laurier et al., 2003; Sprovieri et al., 2003, 2010; Sheu and Mason, 2004; Laurier and Mason, 2007; Soerensen et al., 2010a; Wang et al., 2015).

3.2.2 Spatial distributions of $Hg^P_{2.5}$ and Hg^P_{10}

The concentrations and spatial distribution of $Hg^P_{2.5}$ in the MBL are illustrated in Fig. 4a. The highest $Hg^P_{2.5}$ value (8.3 pg m^{-3}) was observed in the PRE during daytime on 4 September 2015

presumably due to the local human activities. The homogeneous distribution and lower level of $Hg^{P}_{2.5}$ in the open SCS indicated that the $Hg^{P}_{2.5}$ not originated from the land and the SCS suffered less influence from human activities especially in the open sea. This is due to the fact that the majority of air masses in the SCS during this study period came from the seas and oceans. The spatial distribution pattern of $Hg^{P}_{2.5}$ in this study was different from our previous observed patterns in the BS and YS (Wang et al., 2016b), which showed that $Hg^{P}_{2.5}$ concentrations in nearshore area were higher than those in the open sea both in spring and fall mainly due to the outflow of atmospheric Hg^{P} from East China.

The concentrations and spatial distributions of Hg^{P}_{10} in the MBL of the SCS are illustrated in Fig. 4b. We found that the Hg^{P}_{10} concentration was considerably (1–6 times) higher in the PRE than those of other regions of the SCS probably due to the large emissions of anthropogenic Hg in surrounding areas of the PRE. Moreover, the highest $Hg^{P}_{2.1}/Hg^{P}_{10}$ ratio (41 %) was observed in the PRE and coastal sea area of Hainan Island, while lowest ratio (22 %) was observed in the open sea (Fig. 4b). The Hg^{P}_{10} concentrations and $Hg^{P}_{2.1}/Hg^{P}_{10}$ ratios were higher in the nearshore area compared to those in the open sea, demonstrating that coastal sea areas are polluted by anthropogenic Hg to a certain extent. Interestingly, we found the mean $Hg^{P}_{2.1}$ concentration (3.16 ± 2.69 pg m^{-3}, n = 10) measured using the Andersen sampler was comparable to the mean $Hg^{P}_{2.5}$ concentration (3.33 ± 1.89 pg m^{-3}, n = 39) measured using a 47 mm Teflon filter holder (*t*-test, $p > 0.1$). This indicated that the fine Hg^{P} level in the MBL of the SCS was indeed low, and there might be no significant difference in Hg^{P} concentration in the SCS between 12 h and 48 h sampling time.

The concentrations of all size-fractioned Hg^{P} are summarized in Table S1. The size distribution of Hg^{P} in the MBL of the SCS is plotted in Fig. 5. One striking feature is that the three-modal pattern with peaks around <0.4 μm, 0.7–1.1 μm and 5.8–9.0 μm was observed for the size distributions of Hg^{P} in the open sea (Fig. 5a) if we excluded the data in the PRE. The three-modal pattern was more obvious when we consider all the data (Fig. 5b). Generally, the Hg^{P} concentrations in coarse particles were significantly higher than those in fine particles, and $Hg^{P}_{2.1}$ contributed approximately 32 % (22–41 %, see Fig. 4b) to the Hg^{P}_{10} for the whole data, indicating that the coarse mode was the dominant size during this study period. This might be explained by the sources of the air masses. Since air masses dominantly originated from sea and ocean (Figs. S1, S2) and contained high concentrations of sea salts which generally exist in the coarse mode (1–10 μm) (Athanasopoulou et al., 2008; Mamane et al., 2008), the $Hg^{P}_{2.1}/Hg^{P}_{10}$ ratios were generally lower in the SCS compared to those in the BS, YS and ECS (Wang et al., 2016a).

3.3 Dry deposition fluxes of RGM and Hg^{P}

The dry deposition flux of Hg^{P}_{10} was obtained by summing the dry deposition fluxes of each size-fractionated Hg^{P} in the same set. The dry deposition flux of Hg^{P}_{10} is calculated using the following equation: $F = \sum C\mathrm{Hg}^{P} \times V_d$, the F is the dry deposition flux of Hg^{P}_{10} (ng m^{-2} d^{-1}), $C\mathrm{Hg}^{P}$

is the concentration of Hg^P in each size fraction (pg m^{-3}), and V_d is the corresponding dry deposition velocity (cm s^{-1}). In this study, the dry deposition velocities of 0.03, 0.01, 0.06, 0.15 and 0.55 cm s^{-1} (Giorgi, 1988; Pryor et al., 2000; Nho-Kim et al., 2004) were chosen for the following size-fractioned particles: < 0.4, 0.4–1.1, 1.1–2.1, 2.1–5.8 and 5.8–10 μm, respectively (Wang et al., 2016a). The average dry deposition flux of Hg^P_{10} was estimated to be 1.08 ng m^{-2} d^{-1} based on the average concentrations of each size-fractionated Hg^P in the SCS (Table S2), which was lower than those in the BS, YS and ECS (Wang et al., 2016a). The dry deposition velocity of RGM was 4.0–7.6 cm s^{-1} because of its characteristics and rapid uptake by sea salt aerosols followed by deposition (Poissant et al., 2004; Selin et al., 2007). The annual dry deposition fluxes of Hg^P_{10} and RGM to the SCS were calculated to be 1.42 and 27.39–52.05 tons yr^{-1} based on the average Hg^P_{10} and RGM concentrations and the area of the SCS (3.56×10^{12} m^2). The result showed that RGM contributed more than 95 % to the total dry deposition of atmospheric reactive Hg. The annual dry deposition flux of RGM was considerably higher than that of the Hg^P_{10} due to the higher deposition rate and concentrations of RGM.

3.4 Temporal variation of atmospheric Hg

3.4.1 diurnal variation of GEM

The diurnal variation of GEM concentration during the whole study period is illustrated in Fig. 6. It was notable that there was no significant variability of the mean (± SD) GEM concentration in a whole day during this study period, and the GEM concentration dominantly fell in the range of 1.3–1.7 ng m^{-3} (Fig. 6). The statistical result showed that the mean GEM concentration in the daytime (6:00–18:00) (1.49 ± 0.06 pg m^{-3}) was comparable to that in the nighttime (1.51 ± 0.06 pg m^{-3}) (*t*-test, $p > 0.05$). The lower GEM concentrations and smaller variability over the SCS further revealed that the SCS suffered less influence of fresh emissions.

3.4.2 Daily variation of RGM

The average RGM concentrations in the daytime and nighttime are illustrated in Fig. 7. Firstly, it could be found that RGM showed a diurnal variation with higher concentrations in the daytime and lower concentrations in the nighttime during the whole study period. The mean RGM concentration in the daytime (8.0 ± 5.5 pg m^{-3}) was significantly and considerably higher than that in the nighttime (2.2 ± 2.7 pg m^{-3}) (*t*-test, $p < 0.001$). This diurnal pattern was in line with the previous multiple sites studies (Laurier and Mason, 2007; Liu et al., 2007; Engle et al., 2008; Cheng et al., 2014). This is due to the fact that the oxidation of GEM in the MBL must be photochemical, which have been evidenced by the diurnal cycle of RGM (Laurier and Mason, 2007). Another reason is that there was more Br (gas phase) production during daytime (Sander et al., 2003). Figure S3 showed that the RGM concentration in the nighttime was lower than those in corresponding forenoon and afternoon except the measurements in the PRE. This further indicated

that (1) the RGM originated from the photo-oxidation of Hg^0 in the atmosphere and (2) the transfer of RGM to Hg^P due to higher RH and lower air temperature in nighttime (Rutter and Schauer, 2007; Lee et al., 2016).

In addition, we found that the difference in RGM concentration between day and night in the SCS was higher than those in the BS and YS (Wang et al., 2016b), and one possible reason is that the solar radiation and air temperature over the SCS were stronger and higher compared to those over the BS and YS (Wang et al., 2016b) as a result of the specific location of the SCS (tropical sea) and the different sampling season (the SCS: September 2015, the BS and YS: April–May and November 2014). Secondly, it could be found that the higher the RGM concentrations in the daytime, and the higher the RGM concentrations in the nighttime, but the concentrations in daytime were higher than that in the corresponding nighttime throughout the sampling period (see Figs. 7, S3). This is partly because the higher RH and lower air temperature in nighttime were conductive to the removal of RGM (Rutter and Schauer, 2007; Amos et al., 2012). Thirdly, we found that the difference in RGM concentration between different days was large though there was no significantly difference in PAR values (Fig. 7). However, here again divide two kinds of cases: the first kind of circumstance is that the higher RGM in the PRE (day and night) presumably mainly originated from the surrounding human activities (i.e., 4–5 September 2015); the second scenario is that RGM in open waters mainly originated from the in situ oxidation of GEM in the MBL (Soerensen et al., 2010a; Sprovieri et al., 2010). The main reason for the large difference in RGM concentration between different days was that there was large difference in wind speed and RH between different days (see Fig. 2), and the discussion can be found in the following paragraphs.

3.4.3 Daily variation of $Hg^P_{2.5}$

Figure 8 shows the $Hg^P_{2.5}$ concentrations in the daytime and nighttime during the entire study period. The $Hg^P_{2.5}$ value in the daytime (3.4 ± 1.9 pg m^{-3}, n = 20) was slightly but not significantly higher than that in the nighttime (2.4 ± 0.9 pg m^{-3}, n = 19) (*t*-test, $p > 0.1$), and this pattern was consistent with the result of our previous study conducted in the open waters of YS (Wang et al., 2016b). The elevated $Hg^P_{2.5}$ concentrations in the PRE and nearshore area of the Hainan Island (Fig. 4 and Fig. 8) indicated that the nearshore areas were readily polluted due to the anthropogenic Hg emissions, while the low $Hg^P_{2.5}$ level in the open sea further suggested that the open areas of the SCS suffered less anthropogenic Hg^P. Therefore, we postulate that the $Hg^P_{2.5}$ over the open SCS mainly originated from the in situ formation.

During the cruise in the western SCS (16–28 September 2015), we found elevated $Hg^P_{2.5}$ concentrations when the RGM concentrations were high at lower wind speed (e.g., 20–22 September 2015, it was sunny all these days) (see Figs. 2, 7, 8). This is probably due to the transferring of RGM from the gas to the particle phase. In contrast, we found that the $Hg^P_{2.5}$

concentrations were elevated when the RGM concentrations were low at higher wind speed (e.g., 25–27 September 2015, it was cloudy these days, and there was a transitory drizzly on 26 September 2015) (see Figs. 2, 7, 8). On the one hand, high wind speed may increase the levels of halogen atoms (Br and Cl etc.) and sea salt aerosols in the marine atmosphere, which in turn were favorable to the production of RGM and formation of $Hg^{P}_{2.5}$ (Auzmendi-Murua et al., 2014). On the other hand, high wind speed was favorable to the removal of RGM and $Hg^{P}_{2.5}$ in the atmosphere, this was probably the reason for lower RGM and $Hg^{P}_{2.5}$ concentrations during 25–27 September as compared to those observed during 20–22 September (see Fig. 2).

3.5 Relationship between atmospheric Hg and meteorological parameters

Pearson's correlation coefficients were calculated between speciated Hg and meteorological parameters to identify the relationships between them (Table 2). According to the correlation analysis, the $Hg^{P}_{2.5}$ was significantly positively correlated with RGM. Part of the reason was that RGM could be adsorbed by particulate matter under high RGM concentrations and then enhanced the Hg^{P} concentrations. Similarly, the $Hg^{P}_{2.5}$ had a significantly positive correlation with GEM. On the one hand, GEM and Hg^{P} probably originated from the same sources (including but not limited to anthropogenic and oceanic sources) especially in the PRE and nearshore areas. On the other hand, it was probably due to the fact that GEM could be oxidized to form RGM and then Hg^{P}, which might be the reason for the positive but not significant correlation between RGM and GEM since higher GEM level may result in higher RGM level in daytime.

The correlation analysis showed that the $Hg^{P}_{2.5}$ and RGM were all negatively correlated with wind speed and RH (Table 2), and the higher wind speed was favorable to the removal of $Hg^{P}_{2.5}$ over the RGM. This is because the high wind speed might increase the RH levels and then elevated wind speed and RH may accelerate the removal of $Hg^{P}_{2.5}$ and RGM (Cheng et al., 2014; Wang et al., 2016b). Moreover, both the air temperature and PAR were positively correlated with RGM and $Hg^{P}_{2.5}$, and a significantly positive correlation was found between PAR and RGM, indicating that the role of solar radiation played on the production of RGM was more obvious than that on the formation of $Hg^{P}_{2.5}$, which were consistent with the previous study at coastal and marine sites (Mao et al., 2012).

3.6 Sea-air exchange of Hg^{0} in the SCS

The spatial distributions of DGM and Hg^{0} fluxes in the SCS are illustrated in Fig. 9. The DGM concentrations in nearshore area (40−55 pg l^{-1}) were about twice as high as those in the open sea, and this pattern was similar to our previous study conducted in the ECS (Wang et al., 2016c). The DGM concentration in this study varied from 23.0 to 66.8 pg l^{-1} with a mean value of 37.1 ± 9.0 pg l^{-1} (Fig. 9a and Table S3), which was higher than those in other open oceans, such as the Atlantic Ocean (11.6 ± 2.0 pg l^{-1}, Anderson et al., 2011), South Pacific Ocean (9−21 pg l^{-1},

Soerensen et al., 2014), but considerably lower than that in the Minamata Bay (116 ± 76 pg l^{-1}, Marumoto et al., 2015). The mean DGM concentration in the northern SCS (41.3 ± 10.9 pg l^{-1}) was significantly higher than that in the western SCS (33.5 ± 5.0 pg l^{-1}) (*t*-test, $p < 0.01$). The reason was that DGM concentrations in the nearshore areas of the PRE and Hainan Island were higher than those in the western open sea (see Fig. 9a). The DGM in surface seawater of the SCS was supersaturated with a saturation of 501 % to 1468 % with a mean value of 903 ± 208 %, which was approximately two thirds of that measured in the ECS (Wang et al., 2016c). The result indicated that (1) the surface seawater in the SCS was supersaturated with gaseous Hg and (2) Hg^0 evaporated from the surface seawater to the atmosphere during our study period.

The sea-air exchange fluxes of Hg^0 at each station are presented in Table S3, including GEM, DGM, PAR, surface seawater temperature, wind speed and saturation of Hg^0. Sea-air exchange fluxes of Hg^0 in the SCS ranged from 0.40 to 12.71 ng m^{-2} h^{-1} with a mean value of 4.99 ± 3.32 ng m^{-2} h^{-1} (Fig. 9b and Table S3), and which was comparable to the previous measurements obtained in the Mediterranean Sea, the northern SCS and West Atlantic Ocean (Andersson et al., 2007; Fu et al., 2010; Soerensen et al., 2013), but lower than those in polluted marine environments, such as the Minamata Bay, Tokyo Bay and YS (Narukawa et al., 2006; Ci et al., 2011; Marumoto et al., 2015), while higher than those in some open sea environments, such as the Baltic Sea, Atlantic Ocean and South Pacific Ocean (Kuss and Schneider, 2007; Andersson et al., 2011; Kuss et al., 2011; Soerensen et al., 2014). Interestingly, we found the Hg^0 flux near the station 99 were higher than those in open water as a result of higher wind speed (Table S3).

In order to better understand the important role of the SCS, we relate the Hg^0 flux in the SCS to the global estimation, an annual sea-air flux of Hg^0 was calculated based on the assumption that there was no seasonal variation in Hg^0 emission flux from the SCS. The annual emission flux of Hg^0 from the SCS was estimated to be 159.6 tons yr^{-1} assuming the area of the SCS was 3.56 × 10^{12} m^2 (accounting for about 1.0 % of the global ocean area), which constituted about 5.5 % of the global Hg^0 oceanic evasion (Strode et al., 2007; Soerensen et al., 2010b; UNEP, 2013). We attributed the higher Hg^0 flux in the SCS to the specific location of the SCS (tropical sea) and the higher DGM concentrations in the SCS (especially in the northern area). Therefore, the SCS may actually play an important role in the global Hg oceanic cycle. Additionally, we found that the percentage of the annual dry deposition flux of atmospheric reactive Hg to the annual evasion flux of Hg^0 was approximately 18–34 %, indicating that the dry deposition of atmospheric reactive Hg was an important pathway for the atmospheric Hg to the ocean.

4 Conclusions

During the cruise aboard the R/V *Shiyan 3* in September 2015, GEM, RGM and Hg^P were determined in the MBL of the SCS. The GEM level in the SCS was comparable to the background level over the global oceans due to the air masses dominantly originated from seas and oceans.

GEM concentrations were closely related to the sources and movement patterns of air masses during this cruise. Moreover, the speciated atmospheric Hg level in the PRE was significantly higher than those in the open SCS due to the anthropogenic emissions. The Hg^P concentrations in coarse particles were significantly higher than those in fine particles, and the coarse modal was the dominant size though there were three peaks for the size distribution of Hg^P in PM_{10}, indicating that most of the Hg^P_{10} originated from in situ production. There was no significant difference in GEM and $Hg^P_{2.5}$ concentrations between day and night, but RGM concentrations were significantly higher in daytime than in nighttime. RGM was positively correlated with PAR and air temperature, but negatively correlated with wind speed and RH. The DGM concentrations in nearshore areas of the SCS were higher than those in the open sea, and the surface seawater of the SCS was supersaturated with respect to Hg^0. The annual flux of Hg^0 from the SCS accounted for about 5.5 % of the global Hg^0 oceanic evasion though the area of the SCS just represents 1.0 % of the global ocean area, suggesting that the SCS plays an important role in the global Hg cycle. Additionally, the dry deposition of atmospheric reactive Hg was a momentous pathway for the atmospheric Hg to the ocean because it happens all the time.

5 Appendix A

Table A1 List of acronyms and symbols

Abbreviation	Full name
BS	Bohai Sea
YS	Yellow Sea
ECS	East China Sea
SCS	South China Sea
PRE	Pearl River Estuary
MBL	Marine boundary layer
GEM	Gaseous elemental mercury
RGM	Reactive gaseous mercury
TAM	Total atmospheric mercury
$Hg^P_{2.1}$	Particulate mercury in $PM_{2.1}$
$Hg^P_{2.5}$	Particulate mercury in $PM_{2.5}$
Hg^P_{10}	Particulate mercury in PM_{10}
DGM	Dissolved gaseous mercury

Data are available from the first author Chunjie Wang (888wangchunjie888@163.com).

Author contributions. XZ and ZW designed the study. CW and FH organized the mercury measurements. CW performed the data analysis, and wrote the paper. All authors contributed to the manuscript with discussions and comments.

Competing interests. The authors declare that they have no conflict of interest.

Acknowledgments. This research was funded by the National Basic Research Program of China (No. 2013CB430002), National Natural Science Foundation of China (No. 41176066) and "Strategic Priority Research Program" of the Chinese Academy of Sciences, Grant No. XDB14020205. We gratefully acknowledge the open cruise organized by the South China Sea Institute of Oceanology, Chinese Academy of Sciences. The technical assistance of the staff of the R/V *Shiyan 3* is gratefully acknowledged.

References

Ahn, M. C., Kim, B., Holsen, T. M., Yi, S. M., and Han, Y. J.: Factors influencing concentrations of dissolved gaseous mercury (DGM) and total mercury (TM) in an artificial reservoir, Environ. Pollut., 158, 347–355, https://doi.org/10.1016/j.envpol.2009.08.036, 2010.

Amos, H. M., Jacob, D. J., Holmes, C. D., Fisher, J. A., Wang, Q., Yantosca, R. M., Corbitt, E. S., Galarneau, E., Rutter, A. P., Gustin, M. S., Steffen, A., Schauer, J. J., Graydon, J. A., St. Louis, V. L., Talbot, R. W., Edgerton, E. S., Zhang, Y., and Sunderland, E. M.: Gas-particle partitioning of atmopsheric Hg(II) and its effect on global mercury deposition, Atmos. Chem. Phys., 12, 591–603, https://doi.org/10.5194/acp-12-591-2012, 2012.

Andersson, M. E., Gårdfeldt, K., Wängberg, I., Sprovieri, F., Pirrone, N., and Lindqvist, O.: Seasonal and daily variation of mercury evasion at coastal and off shore sites from the Mediterranean Sea, Mar. Chem., 104, 214–226, https://doi.org/10.1016/j.marchem.2006.11.003, 2007.

Andersson, M. E., Sommar, J., Gårdfeldt, K., and Jutterström, S.: Air–sea exchange of volatile mercury in the North Atlantic Ocean, Mar. Chem., 125, 1–7, https://doi.org/10.1016/j.marchem.2011.01.005, 2011.

Angot, H., Barret, M., Magand, O., Ramonet, M., Dommergue, A.: A 2-year record of atmospheric mercury species at a background Southern Hemisphere station on Amsterdam Island, Atmos. Chem. Phys., 14, 11461–11473, https://doi.org/10.5194/acp-14-11461-2014, 2014

Ariya, P. A., Amyot, M., Dastoor, A., Deeds, D., Feinberg, A., Kos, G., Poulain, A., Ryjkov, A., Semeniuk, K., Subir, M., and Toyota, K.: Mercury Physicochemical and Biogeochemical Transformation in the Atmosphere and at Atmospheric Interfaces: A Review and Future Directions, Chem. Rev., 115, 3760–3802, https://doi.org/10.1021/cr500667e, 2015.

Athanasopoulou, E., Tombrou, M., Pandis, S. N., and Russell, A. G.: The role of sea-salt emissions and heterogeneous chemistry in the air quality of polluted coastal areas, Atmos. Chem. Phys., 8, 5755–5769, https://doi.org/10.5194/acp-8-5755-2008, 2008.

Auzmendi-Murua, I., Castillo, Á., and Bozzelli, J. W.: Mercury oxidation via chlorine, bromine, and iodine under atmospheric conditions: Thermochemistry and kinetics, J. Phys. Chem. A, 118, 2959−2975, https://doi.org/10.1021/jp412654s, 2014.

Bowman, K. L., Hammerschmidt, C. R., Lamborg, C. H., and Swarr, G.: Mercury in the North Atlantic Ocean: the U.S. Geotraces zonal and Meridional sections, Deep Sea Res. Part II, 116, 251–261, https://doi.org/10.1016/j.dsr2.2014.07.004, 2015.

Chand, D., Jaffe, D., Prestbo, E., Swartzendruber, P. C., Hafner, W., Weiss-Penzias, P., Kato, S., Takami, A., Hatakeyama, S., and Kajii, Y.: Reactive and particulate mercury in the Asian marine boundary layer, Atmos. Environ., 42, 7988–7996, https://doi.org/10.1016/j.atmosenv.2008.06.048, 2008.

Cheng, I., Zhang, L., Blanchard, P., Graydon, J. A., and St. Louis, V. L.: Source-receptor relationships for speciated atmospheric mercury at the remote Experimental Lakes Area, northwestern Ontario, Canada, Atmos. Chem. Phys., 12, 1903–1922, https://doi.org/10.5194/acp-12-1903-2012, 2012.

Cheng, I., Zhang, L., Blanchard, P., Dalziel, J., Tordon, R., Huang, J., and Holsen, T. M.: Comparisons of mercury sources and atmospheric mercury processes between a coastal and inland site, J. Geophys. Res., 118, 2434–2443, https://doi.org/10.1002/jgrd.50169, 2013.

Cheng, I., Zhang, L., Mao, H., Blanchard, P., Tordon, R., and Dalziel, J.: Seasonal and diurnal patterns of speciated atmospheric mercury at a coastal-rural and a coastal-urban site, Atmos. Environ., 82, 193–205, https://doi.org/10.1016/j.atmosenv.2013.10.016, 2014.

Choi, H. D., Holsen, T. M., and Hopke, P. K.: Atmospheric mercury (Hg) in the Adirondacks: Concentrations and sources, Environ. Sci. Technol., 42, 5644–5653, https://doi.org/10.1021/es7028137, 2008.

Ci, Z., Zhang, X., Wang, Z., Niu, Z., Diao, X., and Wang, S.: Distribution and air–sea exchange of mercury (Hg) in the Yellow Sea, Atmos. Chem. Phys., 11, 2881–2892, https://doi.org/10.5194/acp-11-2881-2011, 2011.

Ci, Z., Wang, C., Wang, Z., and Zhang, X.: Elemental mercury (Hg(0)) in air and surface waters of the Yellow Sea during late spring and late fall 2012: Concentration, spatial-temporal distribution and air/sea flux, Chemosphere, 119, 199–208, https://doi.org/10.1016/j.chemosphere.2014.05.064, 2015.

de Foy, B., Tong, Y., Yin, X., Zhang, W., Kang, S., Zhang, Q., Zhang, G., Wang, X., Schauer, J. J.: First field-based atmospheric observation of the reduction of reactive mercury driven by sunlight, Atmos. Environ., 134, 27-39, https://doi.org/10.1016/j.atmosenv.2016.03.028, 2016.

Draxler, R. R., and Rolph, G. D.: HYSPLITModel access via NOAA ARL READY Website (http://www.arl.noaa.gov/ready/hysplit4.html), NOAA Air Resources Laboratory, Silver Spring, MD, 2012.

Engle, M. A., Tate, M. T., Krabbenhoft, D. P., Kolker, A., Olson, M. L., Edgerton, E. S., DeWild, J. F., and McPherson, A. K.: Characterization and cycling of atmospheric mercury along the central US Gulf Coast, Appl. Geochem., 23, 419–437, https://doi.org/10.1016/j.apgeochem.2007.12.024, 2008.

Feddersen, D. M., Talbot, R., Mao, H., and Sive, B. C.: Size distribution of particulate mercury in marine and coastal atmospheres, Atmos. Chem. Phys., 12, 10899–10909, https://doi.org/10.5194/acp-12-10899-2012, 2012.

Fu, X., Feng, X., Zhang, G., Xu, W., Li, X., Yao, H., Liang, P., Li, J., Sommar, J., Yin, R., and Liu, N.: Mercury in the marine boundary layer and seawater of the South China Sea: Concentrations, sea/air flux, and implication for land outflow, J. Geophys. Res., 115, D06303, https://doi.org/10.1029/2009JD012958, 2010.

Fu, X., Feng, X., Qiu, G., Shang, L., and Zhang, H.: Speciated atmospheric mercury and its potential source in Guiyang, China, Atmos. Environ., 45, 4205–4212, https://doi.org/10.1016/j.atmosenv.2011.05.012, 2011.

Fu, X., Feng, X., Liang, P., Deliger, Zhang, H., Ji, J., and Liu, P.: Temporal trend and sources of speciated atmospheric mercury at Waliguan GAW station, Northwestern China, Atmos. Chem. Phys., 12, 1951–1964, https://doi.org/10.5194/acp-12-1951-2012, 2012.

Gratz, L. E., Ambrose, J. L., Jaffe, D. A., Shah, V., Jaegle, L., Stutz, J., Festa, J., Spolaor, M., Tsai, C., Selin, N. E., Song, S., Zhou, X., Weinheimer, A. J., Knapp, D. J., Montzka, D. D., Flocke, F. M., Campos, T. L., Apel, E., Hornbrook, R., Blake, N. J., Hall, S., Tyndall, G. S., Reeves, M., Stechman, D., and Stell, M.: Oxidation of mercury by bromine in the subtropical Pacific free troposphere, Geophys. Res. Lett., 42, 10494–10502, https://doi.org/10.1002/2015GL066645, 2015.

Giorgi, F.: Dry deposition velocities of atmospheric aerosols as inferred by applying a particle dry deposition parameterisation to a general circulation model, Tellus, 40B, 23–41, https://doi.org/10.1111/j.1600-0889.1988.tb00210.x, 1988.

Gustin, M. S., Huang, J., Miller, M. B., Peterson, C., Jaffe, D. A., Ambrose, J., Finley, B. D., Lyman, S. N., Call, K., Talbot, R., Feddersen, D., Mao, H., and Lindberg, S. E.: Do we understand what the mercury speciation instruments are actually measuring? Results of RAMIX, Environ. Sci. Technol., 47, 7295–7306, https://doi.org/10.1021/es3039104, 2013.

Hedgecock, I. and Pirrone, N.: Mercury and photochemistry in the marine boundary layer-modelling studies suggest the in situ production of reactive gas phase mercury, Atmos. Environ., 35, 3055–3062, https://doi.org/10.1016/S1352-2310(01)00109-1, 2001.

Holmes, C. D., Jacob, D. J., and Yang, X.: Global lifetime of elemental mercury against oxidation by atomic bromine in the free troposphere, Geophys. Res. Lett., 33, L20808, https://doi.org/10.1029/2006gl027176, 2006.

Holmes, C. D., Jacob, D. J., Mason, R. P., and Jaffe, D. A.: Sources and deposition of reactive gaseous mercury in the marine atmosphere, Atmos. Environ., 43, 2278–2285, https://doi.org/10.1016/j.atmosenv.2009.01.051, 2009.

Holmes, C. D., Jacob, D. J., Corbitt, E. S., Mao, J., Yang, X., Talbot, R., and Slemr, F.: Global atmospheric model for mercury including oxidation by bromine atoms, Atmos. Chem. Phys., 10, 12037−12057, https://doi.org/10.5194/acp-10-12037-2010, 2010.

Horowitz, H. M., Jacob, D. J., Zhang, Y., Dibble, T. S., Slemr, F., Amos, H. M., Schmidt, J. A., Corbitt, E. S., Marais, E. A., and Sunderland, E. M.: A new mechanism for atmospheric mercury redox chemistry: implications for the global mercury budget, Atmos. Chem. Phys., 17, 6353-6371, https://doi.org/10.5194/acp-17-6353-2017, 2017.

Horvat, M., Kotnik, J., Logar, M., Fajon, V., Zvonarić, T., and Pirrone, N.: Speciation of mercury in surface and deep-sea waters in the Mediterranean Sea, Atmos. Environ., 37, S93–S108, https://doi.org/10.1016/S1352-2310(03)00249-8, 2003.

Howard, D., Nelson, P. F., Edwards, G. C., Morrison, A. L., Fisher, J. A., Ward, J., Harnwell, J., van der Schoot, M., Atkinson, B., Chambers, S. D., Griffiths, A. D., Werczynski, S., and Williams, A. G.: Atmospheric mercury in the Southern Hemisphere tropics: seasonal and diurnal variations and influence of inter-hemispheric transport, Atmos. Chem. Phys., 17, 11623-11636, https://doi.org/10.5194/acp-17-11623-2017, 2017.

Huang, J., Miller, M. B., Edgerton, E., and Sexauer Gustin, M.: Deciphering potential chemical compounds of gaseous oxidized mercury in Florida, USA, Atmos. Chem. Phys., 17, 1689-1698, https://doi.org/10.5194/acp-17-1689-2017, 2017.

Kim, S. H., Han, Y. J., Holsen, T. M., and Yi, S. M.: Characteristics of atmospheric speciated mercury

concentrations (TGM, Hg(II) and Hg(p)) in Seoul, Korea, Atmos. Environ., 43, 3267–3274, https://doi.org/10.1016/j.atmosenv.2009.02.038, 2009.

Kim, P. R., Han, Y. J., Holsen, T. M., and Yi, S. M.: Atmospheric particulate mercury: Concentrations and size distributions, Atmos. Environ., 61, 94–102, https://doi.org/10.1016/j.atmosenv.2012.07.014, 2012.

Kuss, J.: Water–air gas exchange of elemental mercury: An experimentally determined mercury diffusion coefficient for Hg^0 water–air flux calculations, Limnol. Oceanogr., 59, 1461–1467, https://doi.org/10.4319/lo.2014.59.5.1461, 2014.

Kuss, J., and Schneider, B.: Variability of the gaseous elemental mercury sea-air flux of the Baltic Sea, Environ. Sci. Technol., 41, 8018−8023, https://doi.org/10.1021/es0716251, 2007.

Kuss, J., Zülicke, C., Pohl, C., and Schneider, B.: Atlantic mercury emission determined from continuous analysis of the elemental mercury sea-air concentration difference within transects between 50°N and 50°S, Global Biogeochem. Cycles, 25, GB 3021, https://doi.org/10.1029/2010GB003998, 2011.

Kuss, J., Krüger, S., Ruickoldt, J., and Wlost, K.-P.: High-resolution measurements of elemental mercury in surface water for an improved quantitative understanding of the Baltic Sea as a source of atmospheric mercury, Atmos. Chem. Phys., 18, 4361-4376, https://doi.org/10.5194/acp-18-4361-2018, 2018.

Landis, M. S., Stevens, R. K., Schaedlich, F., and Prestbo, E. M.: Development and characterization of an annular denuder methodology for the measurement of divalent inorganic reactive gaseous mercury in ambient air, Environ. Sci. Technol., 36, 3000–3009, https://doi.org/10.1021/es015887t, 2002.

Laurier, F. J. G., Mason, R. P., Whalin, L., and Kato, S.: Reactive gaseous mercury formation in the North Pacific Ocean's marine boundary layer: A potential role of halogen chemistry, J. Geophys. Res., 108, 4529, https://doi.org/10.1029/2003JD003625, 2003.

Laurier, F., and Mason, R.: Mercury concentration and speciation in the coastal and open ocean boundary layer, J. Geophys. Res., 112, D06302, https://doi.org/10.1029/2006JD007320, 2007.

Lee, G.-S., Kim, P.-R., Han, Y.-J., Holsen, T. M., Seo, Y.-S., and Yi, S.-M.: Atmospheric speciated mercury concentrations on an island between China and Korea: sources and transport pathways, Atmos. Chem. Phys., 16, 4119-4133, https://doi.org/10.5194/acp-16-4119-2016, 2016.

Lindberg, S. E., Brooks, S., Lin, C. J., Scott, K. J., Landis, M. S., Stevens, R. K., Goodsite, M., and Richter, A.: Dynamic oxidation of gaseous mercury in the Arctic troposphere at polar sunrise, Environ. Sci. Technol., 36, 1245–1256, https://doi.org/10.1021/es0111941, 2002.

Liss, P. W., and Slater, P. G.: Flux of gases across the air-sea interface, Nature, 247, 181–184, https://doi.org/10.1038/247181a0, 1974.

Liu, B., Keeler, G. J., Dvonch, J. T., Barres, J. A., Lynam, M. M., Marsik, F. J., and Morgan, J. T.: Temporal variability of mercury speciation in urban air, Atmos. Environ., 41, 1911–1923, https://doi.org/10.1016/j.atmosenv.2006.10.063, 2007.

Liu, B., Keeler, G. J., Dvonch, J. T., Barres, J. A., Lynam, M. M., Marsik, F. J., and Morgan, J. T.: Urban-rural differences in atmospheric mercury speciation, Atmos. Environ., 44, 2013–2023, https://doi.org/10.1016/j.atmosenv.2010.02.012, 2010.

Liu, N., Qiu, G., Landis, M., Feng, X., Fu, X., and Shang, L.: Atmospheric mercury species measured in Guiyang, Guizhou province, southwest China, Atmos. Res., 100, 93–102, https://doi.org/10.1016/j.atmosres.2011.01.002, 2011.

Mamane, Y., Perrino, C., Yossef, O., and Catrambone, M.: Source characterization of fine and coarse particles at the East mediterranean coast, Atmos. Environ., 42, 6114–6130, doi:10.1016/j.atmosenv.2008.02.045, 2008.

Mao, H., Talbot, R., Hegarty, J., and Koermer, J.: Speciated mercury at marine, coastal, and inland sites in New England – Part 2: Relationships with atmospheric physical parameters, Atmos. Chem. Phys., 12, 4181–4206, https://doi.org/10.5194/acp-12-4181-2012, 2012.

Mao, H., Cheng, I., and Zhang, L.: Current understanding of the driving mechanisms for spatiotemporal variations of atmospheric speciated mercury: a review, Atmos. Chem. Phys., 16, 12897–12924, https://doi.org/10.5194/acp-16-12897-2016, 2016.

Mao, H., Hall, D., Ye, Z., Zhou, Y., Felton, D., and Zhang, L.: Impacts of large-scale circulation on urban ambient concentrations of gaseous elemental mercury in New York, USA, Atmos. Chem. Phys., 17, 11655–11671, https://doi.org/10.5194/acp-17-11655-2017, 2017.

Marumoto, K., and Imai, S.: Determination of dissolved gaseous mercury in seawater of Minamata Bay and estimation for mercury exchange across air–sea interface, Mar. Chem., 168, 9–17, https://doi.org/10.1016/j.marchem.2014.09.007, 2015.

Mason, R. P., Choi, A. L., Fitzgerald, W. F., Hammerschmidt, C. R., Lamborg, C. H., Soerensen, A. L., and Sunderland, E. M.: Mercury biogeochemical cycling in the ocean and policy implications, Environ. Res., 119, 101–117, doi:10.1016/j.envres.2012.03.013, 2012.

Mason, R. P., Hammerschmidt, C. R., Lamborg, C. H., Bowman, K. L., Swarr, G. J., and Shelley, R. U.: The air-sea exchange of mercury in the low latitude Pacific and Atlantic Oceans, Deep Sea Res. Part I, 122, 17–28, https://doi.org/10.1016/j.dsr.2017.01.015, 2017.

Narukawa, M., Sakata, M., Marumoto, K., and Asakura, K.: Air-sea exchange of mercury in Tokyo Bay, J. Oceanogr., 62, 249–257, https://doi.org/10.1007/s10872-006-0049-3, 2006.

Nho-Kim, E. Y., Michou, M., and Peuch, V. H.: Parameterization of size-dependent particle dry deposition velocities for global modeling, Atmos. Environ., 38, 1933–1942, https://doi.org/10.1016/j.atmosenv.2004.01.002, 2004.

Poissant, L., Pilote, M., Xu, X., Zhang, H. and Beauvais C.: Atmospheric mercury speciation and deposition in the Bay St. Fran ̧ois wetlands, J. Geophys. Res., 109, D11301, https://doi.org/10.1029/2003JD004364, 2004.

Pryor, S. C., and Sorensen, L. L.: Nitric acid-sea salt reactions: Implications for nitrogen deposition to water surfaces, J. Appl. Meteorol., 39, 725–731, https://doi.org/10.1175/1520-0450-39.5.725, 2000.

Radke, L. F., Friedli, H. R., and Heikes, B. G.: Atmospheric mercury over the NE Pacific during spring 2002: Gradients, residence time, upper troposphere lower stratosphere loss, and long-range transport, J. Geophys. Res., 112, D19305, https://doi.org/10.1029/2005JD005828, 2007.

Read, K. A., Neves, L. M., Carpenter, L. J., Lewis, A. C., Fleming, Z. L., and Kentisbeer, J.: Four years (2011–2015) of total gaseous mercury measurements from the Cape Verde Atmospheric Observatory, Atmos.

669 Chem. Phys., 17, 5393-5406, https://doi.org/10.5194/acp-17-5393-2017, 2017.
670 Rutter, A. P., and Schauer, J. J.: The effect of temperature on the gas–particle partitioning of reactive mercury in
671 atmospheric aerosols, Atmos. Environ., 41, 8647–8657, https://doi.org/10.1016/j.atmosenv.2007.07.024, 2007.
672 Sander, R., Keene, W. C., Pszenny, A. A. P., Arimoto, R., Ayers, G. P., Baboukas, E., Cainey, J. M., Crutzen, P. J.,
673 Duce, R. A., Hönninger, G., Huebert, B. J., Maenhaut, W., Mihalopoulos, N., Turekian, V. C., and Van Dingenen,
674 R., Inorganic bromine in the marine boundary layer: a critical review, Atmos. Chem. Phys., 3, 1301–1336,
675 https://doi.org/10.5194/acp-3-1301-2003, 2003.
676 Schroeder, W. H., and Munthe, J.: Atmospheric mercury – An overview, Atmos. Environ., 32, 809–822,
677 https://doi.org/10.1016/S1352-2310(97)00293-8, 1998.
678 Selin, N. E., Jacob, D. J., Park, R. J., Yantosca, R. M., Strode, S., Jaeglé, L., and Jaffe, D.: Chemical cycling and
679 deposition of atmospheric mercury: Global constraints from observations, J. Geophys. Res., 112, D02308,
680 https://doi.org/10.1029/2006JD007450, 2007.
681 Shah, V., Jaeglé, L., Gratz, L. E., Ambrose, J. L., Jaffe, D. A., Selin, N. E., Song, S., Campos, T. L., Flocke, F. M.,
682 Reeves, M., Stechman, D., Stell, M., Festa, J., Stutz, J., Weinheimer, A. J., Knapp, D. J., Montzka, D. D.,
683 Tyndall, G. S., Apel, E. C., Hornbrook, R. S., Hills, A. J., Riemer, D. D., Blake, N. J., Cantrell, C. A., and
684 Mauldin III, R. L.: Origin of oxidized mercury in the summertime free troposphere over the southeastern US,
685 Atmos. Chem. Phys., 16, 1511-1530, https://doi.org/10.5194/acp-16-1511-2016, 2016.
686 Sheu, G. R., and Mason, R. P.: An examination of the oxidation of elemental mercury in the presence of halide
687 surfaces, J. Atmos. Chem., 48, 107–130, https://doi.org/10.1023/B:JOCH.0000036842.37053.e6, 2004.
688 Slemr, F., Angot, H., Dommergue, A., Magand, O., Barret, M., Weigelt, A., Ebinghaus, R., Brunke, E.-G.,
689 Pfaffhuber, K. A., Edwards, G., Howard, D., Powell, J., Keywood, M., and Wang, F.: Comparison of mercury
690 concentrations measured at several sites in the Southern Hemisphere, Atmos. Chem. Phys., 15, 3125-3133,
691 https://doi.org/10.5194/acp-15-3125-2015, 2015.
692 Soerensen, A. L., Skov, H., Jacob, D. J., Soerensen, B. T., and Johnson, M. S.: Global concentrations of gaseous
693 elemental mercury and reactive gaseous mercury in the marine boundary layer, Environ. Sci. Technol., 44,
694 7425–7430, https://doi.org/10.1021/es903839n, 2010a.
695 Soerensen, A. L., Sunderland, E. M., Holmes, C. D., Jacob, D. J., Yantosca, R. M., Skov, H., Christensen, J. H.,
696 Strode, S. A., and Mason, R. P.: An improved global model for air-sea exchange of mercury: high concentrations
697 over the North Atlantic, Environ. Sci. Technol., 44, 8574–8580, https://doi.org/10.1021/es102032g, 2010b.
698 Soerensen, A. L., Mason, R. P., Balcom, P. H., and Sunderland, E. M.: Drivers of surface ocean mercury
699 concentrations and air–sea exchange in the west Atlantic Ocean, Environ. Sci. Technol., 47, 7757−7765,
700 https://doi.org/10.1021/es401354q, 2013.
701 Soerensen, A. L., Mason, R. P., Balcom, P. H., Jacob, D. J., Zhang, Y., Kuss, J., and Sunderland, E. M.: Elemental
702 mercury concentrations and fluxes in the tropical atmosphere and ocean, Environ. Sci. Technol., 48,
703 11312−11319, https://doi.org/10.1021/es503109p, 2014.
704 Sprovieri, F., Pirrone, N., Gärdfeldt, K., and Sommar, J.: Mercury speciation in the marine boundary layer along a
705 6000 km cruise path around the Mediterranean Sea, Atmos. Environ., 37, S63–S71,

https://doi.org/10.1016/S1352-2310(03)00237-1, 2003.

Sprovieri, F., and Pirrone, N.: Spatial and temporal distribution of atmospheric mercury species over the Adriatic Sea, Environ. Fluid Mech., 8, 117–128, https://doi.org/10.1007/s10652-007-9045-4, 2008.

Sprovieri, F., Hedgecock, I. M., and Pirrone, N.: An investigation of the origins of reactive gaseous mercury in the Mediterranean marine boundary layer, Atmos. Chem. Phys., 10, 3985–3997, https://doi.org/10.5194/acp-10-3985-2010, 2010.

Steffen, A., Lehnherr, I., Cole, A., Ariya, P., Dastoor, A., Durnford, D., Kirk, J., and Pilote, M.: Atmospheric mercury measurements in the Canadian Arctic Part 1: A review of recent field measurements, Sci. Total Environ., 509–510, 3–15, https://doi.org/10.1016/j.scitotenv.2014.10.109, 2015.

Strode, S. A., Jaegl é, L., Selin, N. E., Jacob, D. J., Park, R. J., Yantosca, R. M., Mason, R. P., and Slemr, F.: Air-sea exchange in the global mercury cycle, Global Biogeochem. Cycles, 21, GB1017, https://doi.org/10.1029/2006GB002766, 2007.

Tseng, C. M., Liu, C. S., and Lamborg, C.: Seasonal changes in gaseous elemental mercury in relation to monsoon cycling over the northern South China Sea, Atmos. Chem. Phys., 12, 7341–7350, https://doi.org/10.5194/acp-12-7341-2012, 2012.

UNEP: Global Mercury Assessment: Sources, Emissions, Releases and Environmental Transport, UNEP Chemicals Branch, Geneva, Switzerland, 2013.

Valente, R. J., Shea, C., Humes, K. L., and Tanner, R. L.: Atmospheric mercury in the Great Smoky Mountains compared to regional and global levels, Atmos. Environ., 41, 1861–1873, https://doi.org/10.1016/j.atmosenv.2006.10.054, 2007.

Wang, Y. Q., Zhang, X. Y., and Draxler, R. R.: TrajStat: GIS-based software that uses various trajectory statistical analysis methods to identify potential sources from long-term air pollution measurement data, Environ. Model. Softw., 28, 938–939, https://doi.org/10.1016/j.envsoft.2009.01.004, 2009.

Wang, S., Schmidt, J. A., Baidar, S., Coburn, S., Dix, B., Koenig, T. K., Apel, E., Bowdalo, D., Campos, T. L., Eloranta, E., Evans, M. J., DiGangi, J. P., Zondlo, M. A., Gao, R. S., Haggerty, J. A., Hall, S. R., Hornbrook, R. S., Jacob, D., Morley, B., Pierce, B., Reeves, M., Romashkin, P., ter Schure, A., and Volkamer, R.: Active and widespread halogen chemistry in the tropical and subtropical free troposphere, Proc. Natl. Acad. Sci. U.S.A., 112, 9281–9286, https://doi.org/10.1073/pnas.1505142112, 2015.

Wang, C., Wang, Z., Ci, Z., Zhang, X., and Tang, X.: Spatial-temporal distributions of gaseous element mercury and particulate mercury in the Asian marine boundary layer, Atmos. Environ., 126, 107–116, https://doi.org/10.1016/j.atmosenv.2015.11.036, 2016a.

Wang, C., Ci, Z., Wang, Z., Zhang, X., and Guo, J.: Speciated atmospheric mercury in the marine boundary layer of the Bohai Sea and Yellow Sea, Atmos. Environ., 131, 360–370, https://doi.org/10.1016/j.atmosenv.2016.02.021, 2016b.

Wang, C., Ci, Z., Wang, Z., and Zhang, X.: Air-sea exchange of gaseous mercury in the East China Sea, Environ. Pollut., 212, 535–543, https://doi.org/10.1016/j.envpol.2016.03.016, 2016c.

Wanninkhof, R.: Relationship between wind speed and gas exchange over the ocean, J. Geophys. Res., 97,

7373–7382, https://doi.org/10.1029/92JC00188, 1992.

Witt, M. L. I., Mather, T. A., Baker, A. R., De Hoog, J. C. M., and Pyle, D. M.: Atmospheric trace metals over the south-west Indian Ocean: Total gaseous mercury, aerosol trace metal concentrations and lead isotope ratios, Mar. Chem., 121, 2–16, https://doi.org/10.1016/j.marchem.2010.02.005, 2010.

Xu, L., Chen, J., Yang, L., Niu, Z., Tong, L., Yin, L., and Chen, Y.: Characteristics and sources of atmospheric mercury speciation in a coastal city, Xiamen, China, Chemosphere, 119, 530–539, https://doi.org/10.1016/j.chemosphere.2014.07.024, 2015.

Ye, Z., Mao, H., Lin, C.-J., and Kim, S. Y.: Investigation of processes controlling summertime gaseous elemental mercury oxidation at midlatitudinal marine, coastal, and inland sites, Atmos. Chem. Phys., 16, 8461–8478, https://doi.org/10.5194/acp-16-8461-2016, 2016.

Zhu, J., Wang, T., Talbot, R., Mao, H., Yang, X., Fu, C., Sun, J., Zhuang, B., Li, S., Han, Y., and Xie, M.: Characteristics of atmospheric mercury deposition and size-fractionated particulate mercury in urban Nanjing, China, Atmos. Chem. Phys., 14, 2233–2244, https://doi.org/10.5194/acp-14-2233-2014, 2014.

Figures and Tables

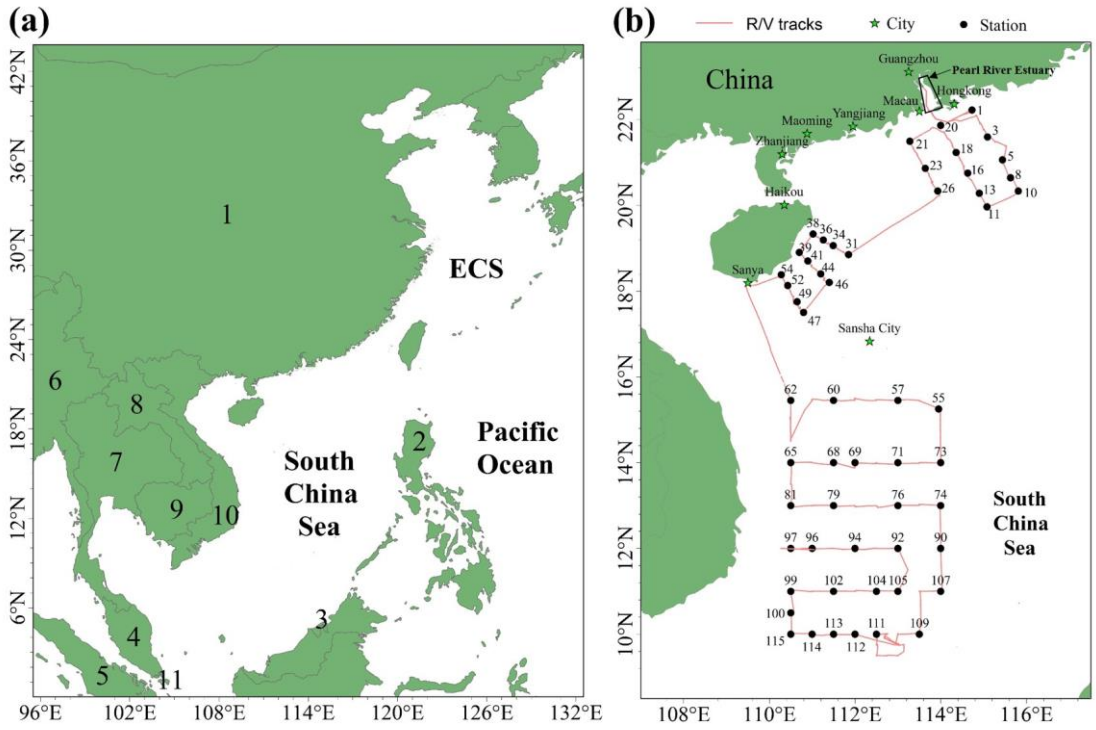

Figure 1. Map of the South China Sea (a) (1: China, 2: Philippines, 3: Brunei, 4: Malaysia, 5: Indonesia, 6: Myanmar, 7: Thailand, 8: Laos, 9: Cambodia, 10: Vietnam, 11: Singapore). The locations of the Pearl River Estuary (PRE), DGM sampling stations and R/V tracks (b). It should be noted that the black solid points represent the sampling stations, and the number near the black solid point represents the name of the station.

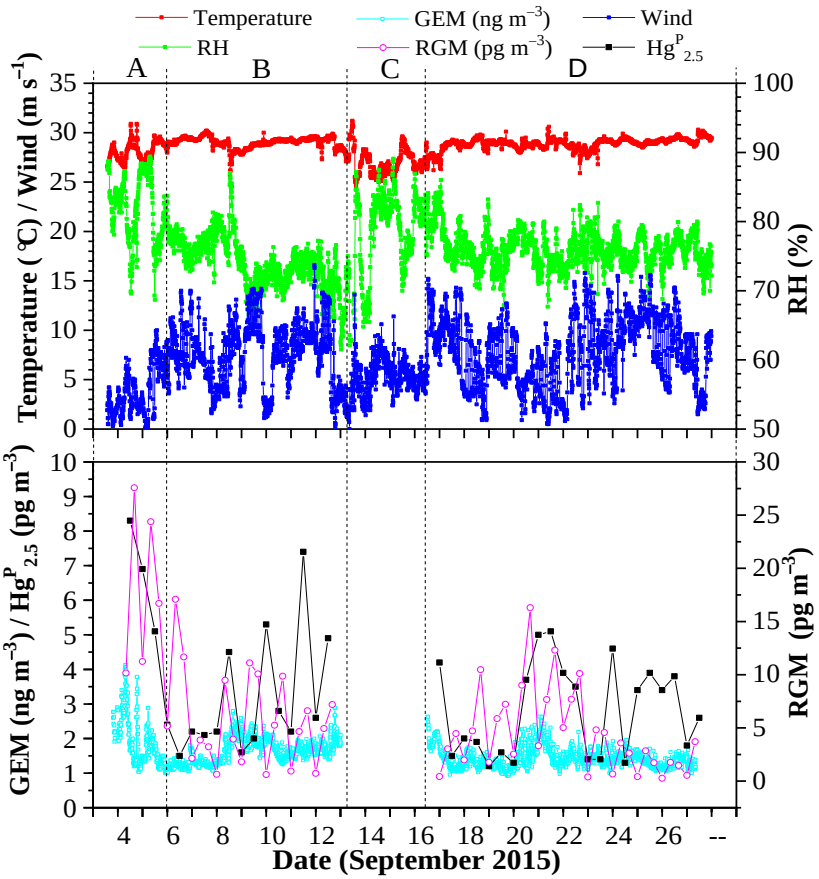

Figure 2. Time (local time) series of GEM, $Hg^{P}_{2.5}$, RGM and some meteorological parameters, including relative humidity (RH), air temperature and wind speed ("A" represents the data measured in the PRE, "B" represents the data measured in the northern SCS, "C" represents the data obtained in the port of Sanya, "D" represents the data measured in the western SCS). It was rainy day on the days of 8 and 26 September 2015.

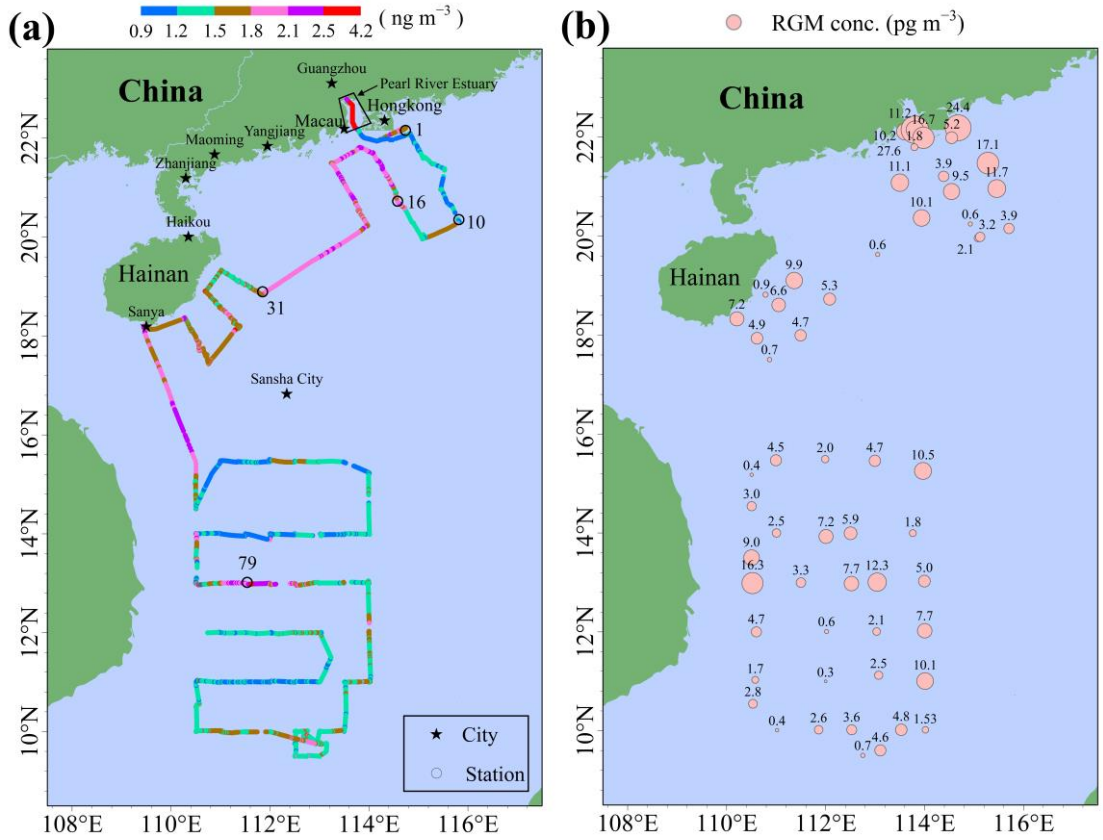

770

771 **Figure 3.** The concentrations and spatial distributions of GEM (a) and RGM (b) in the MBL of the

772 SCS.

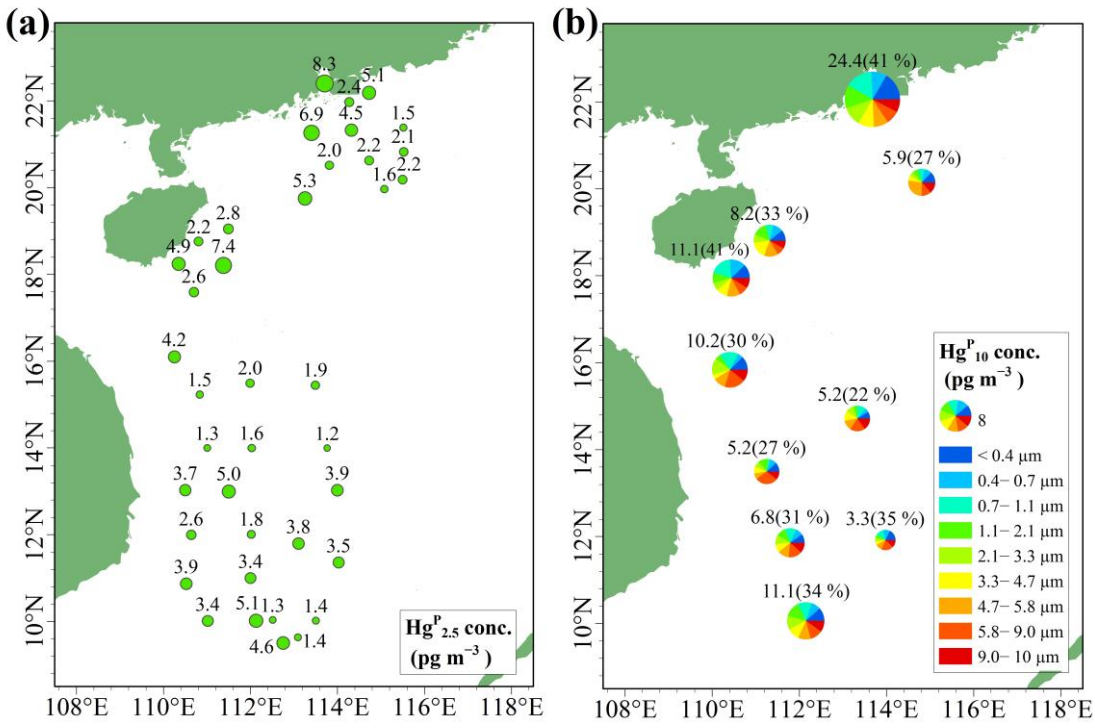

773

774 **Figure 4.** Spatial distributions of $Hg^{P}_{2.5}$ (a) and Hg^{P}_{10} ($Hg^{P}_{2.1}$/Hg^{P}_{10} ratio) (b) in the MBL of the

775 SCS. $Hg^{P}_{2.5}$, $Hg^{P}_{2.1}$ and Hg^{P}_{10} denote the Hg^{P} in $PM_{2.5}$, $PM_{2.1}$ and PM_{10}, respectively.

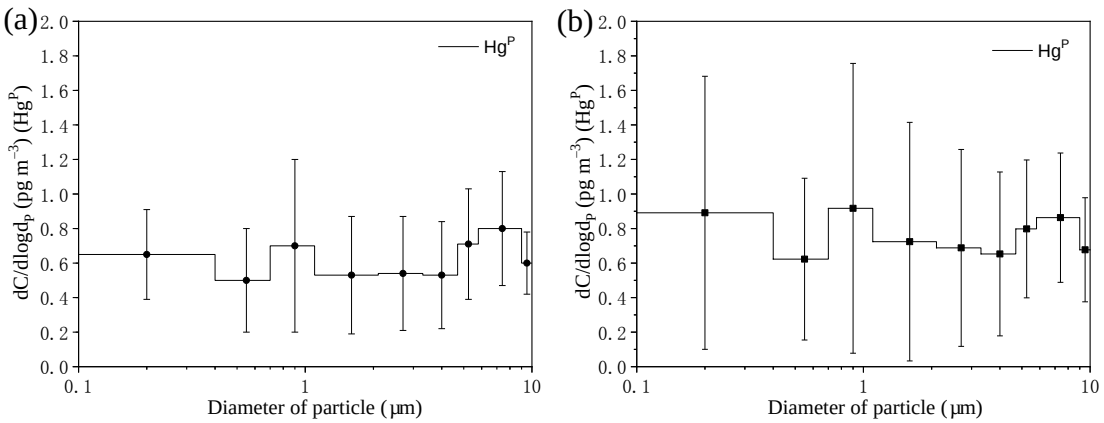

776

777 **Figure 5.** Size distributed concentrations of Hg^P (PM_{10}) in the MBL of the SCS, (a) represents all
778 the data excepting the measurements in the PRE; (b) represents all the data. The data shown are
779 the mean and standard error.

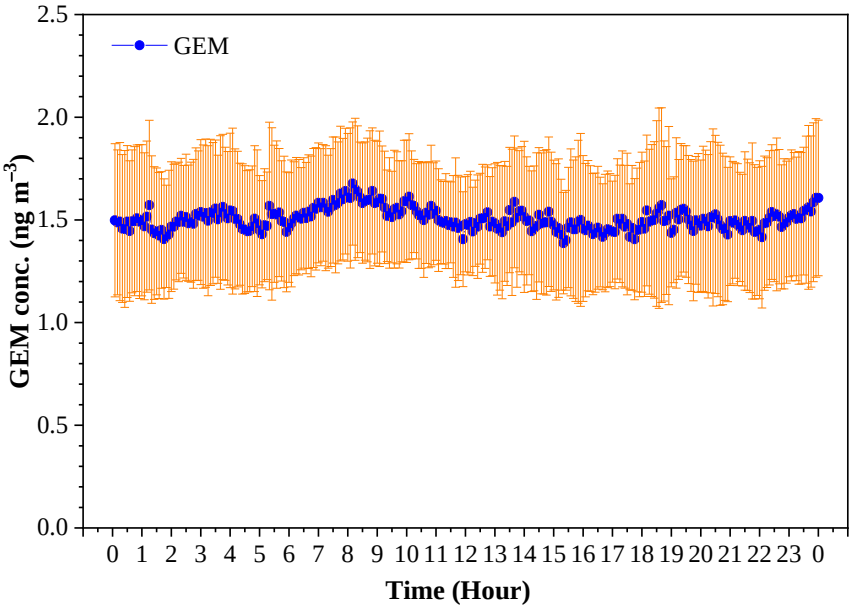

780

781 **Figure 6.** Diurnal variation of GEM concentration (mean ± SD) over the SCS.

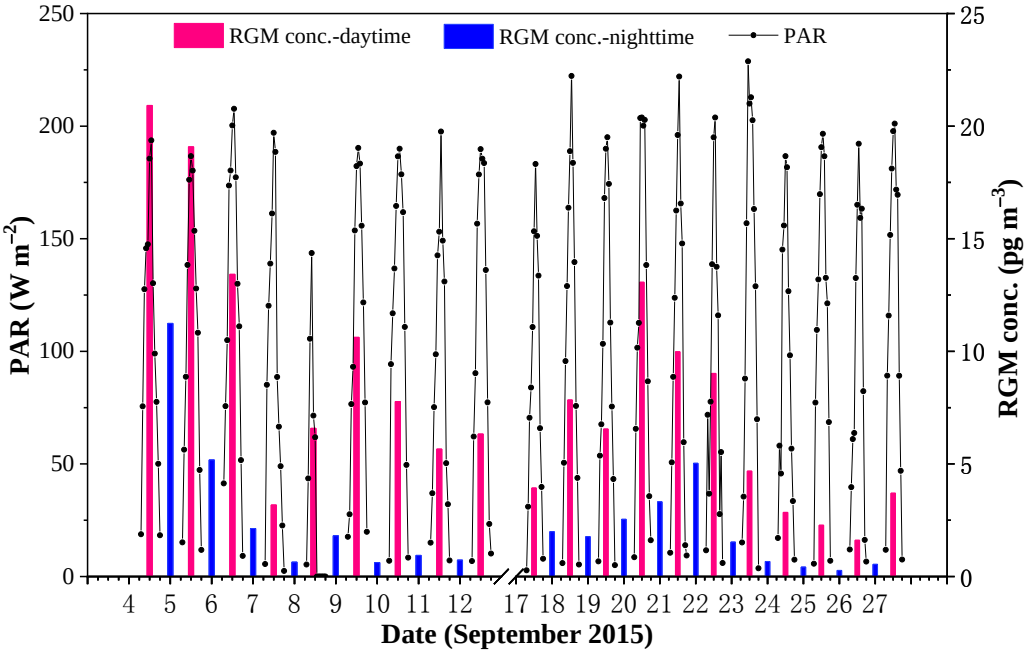

782

783 **Figure 7.** Daily variation of RGM concentration over the SCS.

784

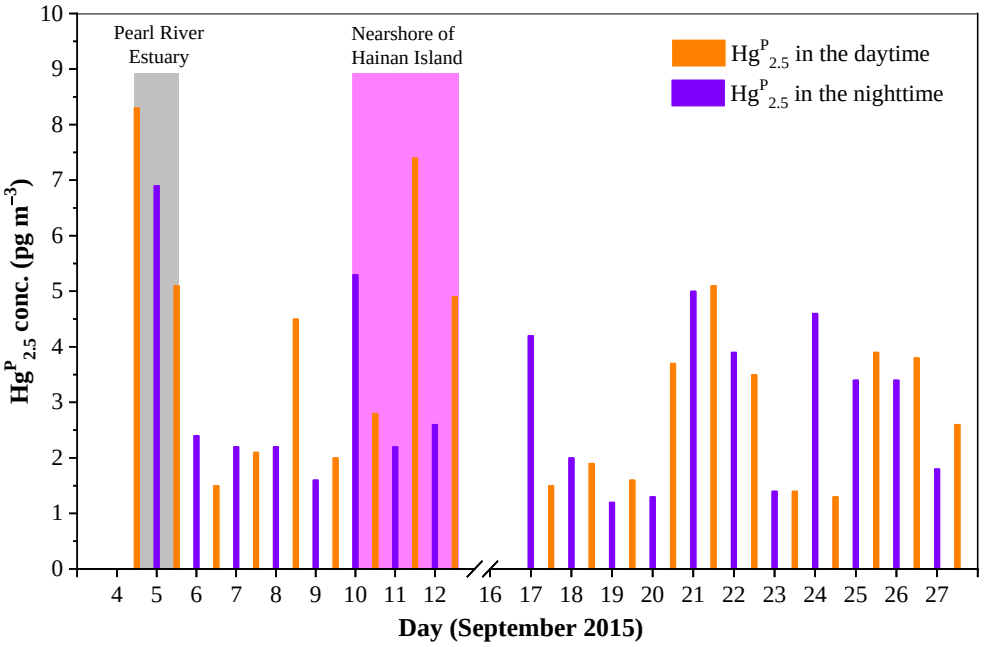

785

786 **Figure 8.** Daily variation of $Hg^{P}_{2.5}$ in the MBL of the SCS. The light gray area represents the data

787 in the PRE, while the light magenta area represents the data in the nearshore area of the Hainan

788 Island.

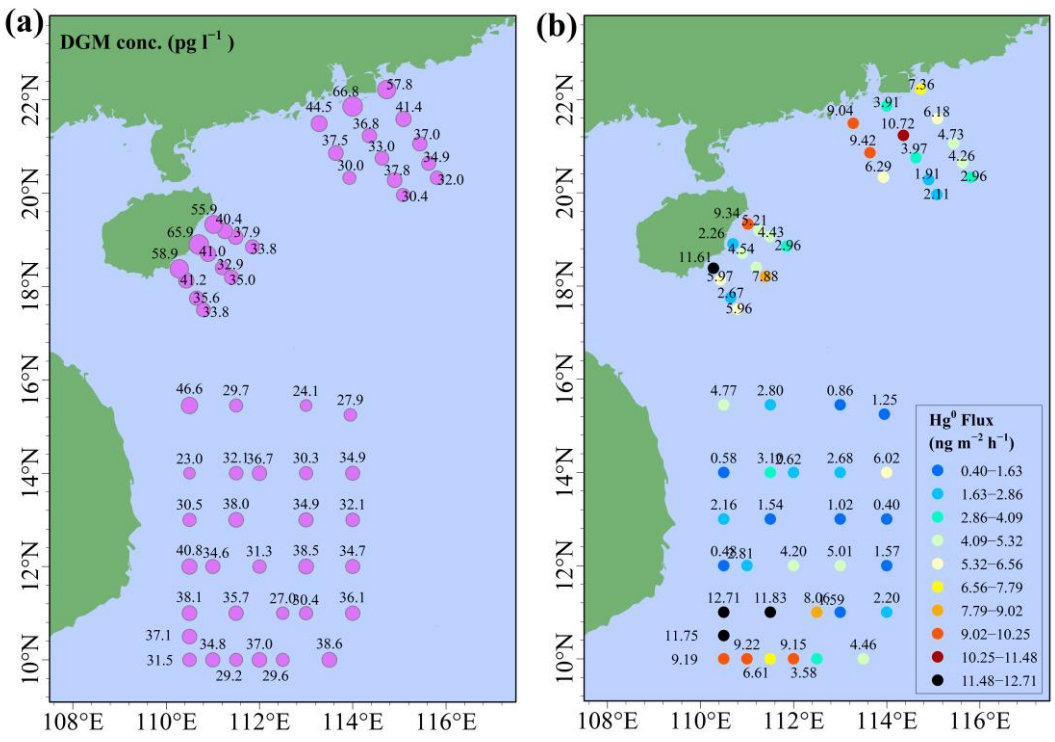

Figure 9. DGM concentrations (a) and sea-air exchange flux of Hg^0 (b) in the SCS.

Table 1. The GEM, $Hg^P_{2.5}$ and RGM concentrations in this study and other literature.

Location		Classification	Sampling time	GEM (ng m^{-3})	$Hg^P_{2.5}$ (pg m^{-3})	RGM (pg m^{-3})	Reference
China	SCS	Sea	2015	1.52 ± 0.32	3.2 ± 1.8	6.1 ± 5.8	This study
	BS and YS	Sea	2014 (Spring)	2.03 ± 0.72	11.3 ± 18.5	2.5 ± 1.7	Wang et al., 2016a, b
	BS and YS	Sea	2014 (Fall)	2.09 ± 1.58	9.0 ± 9.0	4.3 ± 2.5	Wang et al., 2016a, b
	YS	Sea	2010 (Summer)	2.61 ± 0.50	NA[a]	NA	Ci et al., 2011
	YS	Sea	2012 (Spring)	1.86 ± 0.40	NA	NA	Ci et al., 2015
	YS	Sea	2012 (Fall)	1.84 ± 0.50	NA	NA	Ci et al., 2015
	ECS	Sea	2013 (Summer)	1.61 ± 0.32	NA	NA	Wang et al., 2016c
	ECS	Sea	2013 (Fall)	2.20 ± 0.58	NA	NA	Wang et al., 2016c
	Northern SCS	Sea	2007	2.62 ± 1.13	NA	NA	Fu et al., 2010
	Northern SCS	Sea	2003–2005	2.8 –5.7	NA	NA	Tseng et al., 2012
	Nam Co	lake	2014–2015	0.95 ± 0.37	0.85 ± 2.91	49.0 ± 60.3	de Foy et al., 2016
	Xiamen	Coastal urban	2012–2013	3.50	61.05	174.41	Xu et al., 2015
Japan	Okinawa Island	Ocean	2004	2.04 ± 0.38	3.0 ± 2.5	4.5 ± 5.4	Chand et al., 2008
Korea	Seoul	Urban	2005–2006	3.22 ± 2.10	23.9 ± 19.6	27.2 ± 19.3	Kim et al., 2009
USA	Weeks Bay	Coast	2005–2006	1.6 ± 0.3	2.7 ± 3.4	4.0 ± 7.5	Engle et al., 2008
Canada	Ontario Lake	Remote area	2005–2006	1.57 ± 0.22	4.42 ± 3.67	0.99 ± 1.89	Cheng et al., 2012
	Nova Scotia	Coast	2010–2011	1.67 ± 1.01	2.32 ± 3.09	2.07 ± 3.35	Cheng et al., 2013
	Nova Scotia	Coast-rural	2010–2011	1.38 ± 0.20	3.5 ± 4.5	0.4 ± 1.0	Cheng et al., 2014
Australia	ATARS[b]	Coast	2014-2015	0.95 ± 0.12	NA	NA	Howard et al., 2017
South-west India Ocean		Ocean	2007	1.24 ± 0.06	NA	NA	Witt et al., 2010
North Atlantic Ocean		Ocean	2003	1.63 ± 0.08	NA	5.9 ± 4.9	Laurier et al., 2007
West Atlantic Ocean		Ocean	2008–2010	1.4–1.5	NA	NA	Soerensen et al., 2013
North Pacific Ocean		Ocean	2002	2.5	NA	9.5	Laurier et al., 2003
Pacific Ocean		Ocean	2011	1.15–1.32	NA	NA	Soerensen et al., 2014
Mediterranean Sea		Sea	2000	1.9 ± 1.0	NA	7.9	Sprovieri et al., 2003
Global Ocean		Ocean	2006–2007	1.53 ± 0.58	NA	3.1 ± 11.0	Soerensen et al., 2010a
Adriatic Sea		Ocean	2004	1.6 ± 0.4	4.5 ± 8.0	6.7 ± 11.7	Sprovieri and Pirrone, 2008
Amsterdam Island		Ocean	2012–2013	1.03 ± 0.08	0.67	0.34	Angot et al., 2014

[a] NA: No data available.

[b] ATARS: Australian Tropical Atmospheric Research Station.

Table 2. Correlation coefficients for speciated atmospheric Hg and meteorological parameters (one asterisk denotes significant correlation in $p < 0.05$, double asterisks denotes significant correlation in $p < 0.01$).

Speciation	GEM		RGM		$Hg^{P}_{2.5}$		Wind speed		Air temperature		RH		PAR	
	p	*r*	*p*	*r*	*p*	*r*	*p*	*r*	*p*	*r*	*p*	*r*	*p*	*r*
RGM	0.069	0.294			< 0.01	0.453**	0.123	–0.251	0.053	0.313	0.065	–0.299	< 0.01	0.638**
$Hg^{P}_{2.5}$	< 0.01	0.539**	< 0.01	0.453**			0.037	–0.335*	0.621	0.082	0.434	–0.129	0.432	0.130